

Nonequilibrium entropy limiters in lattice Boltzmann methods¹

R. A. Brownlee, A. N. Gorban^{*}, J. Levesley

Department of Mathematics, University of Leicester, Leicester LE1 7RH, UK

Abstract

We construct a system of nonequilibrium entropy limiters for the lattice Boltzmann methods (LBM). These limiters erase spurious oscillations without blurring of shocks, and do not affect smooth solutions. In general, they do the same work for LBM as flux limiters do for finite differences, finite volumes and finite elements methods, but for LBM the main idea behind the construction of nonequilibrium entropy limiter schemes is to transform a field of a scalar quantity — nonequilibrium entropy. There are two families of limiters: (i) based on restriction of nonequilibrium entropy (entropy “trimming”) and (ii) based on filtering of nonequilibrium entropy (entropy filtering). The physical properties of LBM provide some additional benefits: the control of entropy production and accurate estimate of introduced artificial dissipation are possible. The constructed limiters are tested on classical numerical examples: 1D athermal shock tubes with an initial density ratio 1:2 and the 2D lid-driven cavity for Reynolds numbers Re between 2000 and 7500 on a coarse 100×100 grid. All limiter constructions are applicable for both entropic and non-entropic quasiequilibria.

Key words: lattice Boltzmann method, numerical regularisation, entropy

PACS: 47.11.Qr, 47.20.-k, 47.11.-j, 51.10.+y

1 Introduction

In 1959, S.K. Godunov [17] demonstrated that a (linear) scheme for a PDE could not, at the same time, be monotone and second order accurate. Hence,

^{*} Corresponding author.

Email addresses: `r.brownlee@mcs.le.ac.uk` (R. A. Brownlee),
`a.gorban@mcs.le.ac.uk` (A. N. Gorban), `j.levesley@mcs.le.ac.uk`
(J. Levesley).

¹ This work is supported by EPSRC grant number GR/S95572/01.

we should choose between spurious oscillation in high order non-monotone schemes and additional dissipation in first order schemes. Flux limiter schemes are invented to combine high resolution schemes in areas with smooth fields and first order schemes in areas with sharp gradients.

The idea of flux limiters can be illustrated by computation of the flux $F_{0,1}$ of the conserved quantity u between a cell marked by 0 and one of two its neighbour cells marked by ± 1 :

$$F_{0,1} = (1 - \phi(r))f_{0,1}^{\text{low}} + \phi(r)f_{0,1}^{\text{high}},$$

where $f_{0,1}^{\text{low}}$, $f_{0,1}^{\text{high}}$ are low and high resolution scheme fluxes, respectively, $r = (u_0 - u_{-1})/(u_1 - u_0)$, and $\phi(r) \geq 0$ is a flux limiter function. For r close to 1, the flux limiter function $\phi(r)$ should be also close to 1.

Many flux limiter schemes have been invented during the last two decades [43]. No particular limiter works well for all problems, and a choice is usually made on a trial and error basis.

Below are several examples of flux limiter functions:

$$\begin{aligned}\phi_{mm}(r) &= \max[0, \min(r, 1)] \quad (\text{minmod, [36]}); \\ \phi_{os}(r) &= \max[0, \min(r, \beta)], \quad (1 \leq \beta \leq 2) \quad (\text{Osher, [10]}); \\ \phi_{mc}(r) &= \max[0, \min(2r, 0.5(1+r), 2)] \quad (\text{monotonised central [42]}); \\ \phi_{sb}(r) &= \max[0, \min(2r, 1), \min(r, 2)] \quad (\text{superbee, [36]}); \\ \phi_{sw}(r) &= \max[0, \min(\beta r, 1), (r, \beta)], \quad (1 \leq \beta \leq 2) \quad (\text{Sweby, [40]}).\end{aligned}$$

The lattice Boltzmann method has been proposed as a discretization of Boltzmann's kinetic equation and is now in wide use in fluid dynamics and beyond (for an introduction and review see [38]). Instead of fields of moments M , the lattice Boltzmann method operates with fields of discrete distributions f . This allows us to construct very simple limiters that do not depend on slopes or gradients.

All the limiters we construct are based on the representation of distributions f in the form:

$$f = f^* + \|f - f^*\| \frac{f - f^*}{\|f - f^*\|},$$

where f^* is the correspondent quasiequilibrium (conditional equilibrium) for given moments M , $f - f^*$ is the nonequilibrium “part” of the distribution, which is represented in the form “norm×direction” and $\|f - f^*\|$ is the norm of that nonequilibrium component (usually this is the entropic norm). Limiters change the norm of the nonequilibrium component $f - f^*$, but do not touch its direction or the equilibrium. In particular, limiters do not change the

macroscopic variables, because moments for f and f^* coincide. All limiters we use are transformations of the form

$$f \mapsto f^* + \phi \times (f - f^*) \quad (1)$$

with $\phi > 0$. If $f - f^*$ is too big, then the limiter should decrease its norm.

The outline of the paper is as follows. In Sec. 2 we introduce the notions and notations from lattice Boltzmann theory we need, in Sec. 3 we elaborate the idea of entropic limiters in more detail and construct several nonequilibrium entropy limiters for LBM, in Sec. 4 some numerical experiments are described:

- (1) 1D athermal shock tube examples;
- (2) steady state vortex centre locations and observation of first Hopf bifurcation in 2D lid-driven cavity flow.

Concluding remarks are given in Sec. 5.

2 Background

The essence of lattice Boltzmann methods was formulated by S. Succi in the following maxim: “Nonlinearity is local, non-locality is linear”². We should even strengthen this statement. Non-locality (a) is linear; (b) is exactly and explicitly solvable for all time steps; (c) space discretization is an exact operation.

The lattice Boltzmann method is a discrete velocity method. The finite set of velocity vectors $\{\mathbf{v}_i\}$ ($i = 1, \dots, m$) is selected, and a fluid is described by associating, with each velocity \mathbf{v}_i , a single-particle distribution function $f_i = f_i(\mathbf{x}, t)$ which is evolved by advection and interaction (collision) on a fixed computational lattice. The values f_i are named *populations*. If we look at all lattice Boltzmann models, one finds that there are two steps: free flight for time δt and a local collision operation.

The free flight transformation for continuous space is

$$f_i(\mathbf{x}, t + \delta t) = f_i(\mathbf{x} - \mathbf{v}_i \delta t, t).$$

After the free flight step the collision step follows:

$$f_i(\mathbf{x}) \mapsto F_i(\{f_j(\mathbf{x})\}), \quad (2)$$

² S. Succi, “Lattice Boltzmann at all-scales: from turbulence to DNA translocation”, Mathematical Modelling Centre Distinguished Lecture, University of Leicester, Leicester UK, 15th November 2006.

or in the vector form

$$f(\mathbf{x}) \mapsto F(f(\mathbf{x})).$$

Here, the *collision operator* F is the set of functions $F_i(\{f_j\})$ ($i = 1, \dots, m$). Each function F_i depends on all f_j ($j = 1, \dots, m$): new values of the populations f_i at a point \mathbf{x} are known functions of all previous population values at the same point.

The lattice Boltzmann chain “free flight \rightarrow collision \rightarrow free flight \rightarrow collision \dots ” can be exactly restricted onto any space lattice which is invariant with respect to space shifts of the vectors $\mathbf{v}_i \delta t$ ($i = 1, \dots, m$). Indeed, free flight transforms the population values at sites of the lattice into the population values at sites of the same lattice. The collision operator (2) acts pointwise at each lattice site separately. Much effort has been applied to answer the questions: “how does the lattice Boltzmann chain approximate the transport equation for the moments M ?”, and “how does one construct the lattice Boltzmann model for a given macroscopic transport phenomenon?” (a review is presented in book [38]).

In our paper we propose a universal construction of limiters for all possible collision operators, and the detailed construction of $F_i(\{f_j\})$ is not important for this purpose. The only part of this construction we use is the local equilibria (sometimes these states are named conditional equilibria, quasiequilibria, or even simpler, equilibria).

The lattice Boltzmann models should describe the macroscopic dynamic, i.e., the dynamic of macroscopic variables. The macroscopic variables $M_\ell(\mathbf{x})$ are some linear functions of the population values at the same point: $M_\ell(\mathbf{x}) = \sum_i m_{\ell i} f_i(\mathbf{x})$, or in the vector form, $M(\mathbf{x}) = m(f(\mathbf{x}))$. The macroscopic variables are invariants of collisions:

$$\sum_i m_{\ell i} f_i = \sum_i m_{\ell i} F_i(\{f_j\}) \quad (\text{or } m(f) = m(F(f))).$$

The standard example of the macroscopic variables are hydrodynamic fields (density–velocity–energy density): $\{n, n\mathbf{u}, E\}(\mathbf{x}) := \sum_i \{1, \mathbf{v}_i, v_i^2/2\} f_i(\mathbf{x})$. But this is not an obligatory choice. If we would like to solve, by LBM methods, the Grad equations [22] or some extended thermodynamic equations [25], we should extend the list of moments (but, at the same time, we should be ready to introduce more discrete velocities for a proper description of these extended moment systems). On the other hand, the athermal lattice Boltzmann models with a shortened list of macroscopic variables $\{n, n\mathbf{u}\}$ are very popular.

The quasiequilibrium is the positive fixed point of the collision operator for the given macroscopic variables M . We assume that this point exists, is unique and depends smoothly on M . For the quasiequilibrium population vector for given M we use the notation f_M^* , or simply f^* , if the correspondent value of

M is obvious. We use Π^* to denote the equilibration projection operation of a distribution f into the corresponding quasiequilibrium state:

$$\Pi^*(f) = f_{m(f)}^*.$$

For some of the collision models an entropic description of equilibrium is possible: an entropy density function $S(f)$ is defined and the quasiequilibrium point f_M^* is the entropy maximiser for given M [26,39].

As a basic example we shall consider the lattice Bhatnagar–Gross–Krook (LBGK) model with overrelaxation (see, e.g., [3,12,23,28,38]). The LBGK collision operator is

$$F(f) := \Pi^*(f) + (2\beta - 1)(\Pi^*(f) - f), \quad (3)$$

where $\beta \in [0, 1]$. For $\beta = 0$, LBGK collisions do not change f , for $\beta = 1/2$ these collisions act as equilibration (this corresponds to the Ehrenfests' coarse graining [15] further developed in [14,19,20]), for $\beta = 1$, LBGK collisions act as a point reflection with the center at the quasiequilibrium $\Pi^*(f)$.

It is shown [8] that under some stability conditions and after an initial period of relaxation, the simplest LBGK collision with overrelaxation [23,38] provides second order accurate approximation for the macroscopic transport equation with viscosity proportional to $\delta t(1 - \beta)/\beta$.

The entropic LBGK (ELBM) method [5,20,26,39] differs in the definition of (3): for $\beta = 1$ it should conserve the entropy, and in general has the following form:

$$F(f) := (1 - \beta)f + \beta\tilde{f}, \quad (4)$$

where $\tilde{f} = (1 - \alpha)f + \alpha\Pi^*(f)$. The number $\alpha = \alpha(f)$ is chosen so that the constant entropy condition is satisfied: $S(f) = S(\tilde{f})$. For LBGK (3), $\alpha = 2$. Of course, for ELBM the entropic definition of quasiequilibrium should be valid.

In the low-viscosity regime, LBGK suffers from numerical instabilities which readily manifest themselves as local blow-ups and spurious oscillations.

The LBM experiences the same spurious oscillation problems near sharp gradients as high order schemes do. The physical properties of the LBM schemes allows one to construct new types of limiters: the nonequilibrium entropy limiters. In general, they do the same work for LBM as flux limiters do for finite differences, finite volumes and finite elements methods, but for LBM the main idea behind the construction of nonequilibrium entropy limiter schemes is to limit a scalar quantity — nonequilibrium entropy (and not the vectors or tensors of spatial derivatives, as it is for flux limiters). These limiters introduce some additional dissipation, but all this dissipation could easily be evaluated through analysis of nonequilibrium entropy production.

Two examples of such limiters have been recently proposed: the positivity rule [6,31,41] and the Ehrenfests' regularisation [7]. The positivity rule just provides positivity of distributions: if a collision step produces negative populations, then the positivity rule returns them to the boundary of positivity. In the Ehrenfests' regularisation, one selects the k sites with highest nonequilibrium entropy (the difference between entropy of the state f and entropy of the corresponding quasiequilibrium state f^* at a given space point) that exceed a given threshold and equilibrates the state in these sites.

The positivity rule and Ehrenfests' regularisation provide rare, intense and localised corrections. It is easy and also computationally cheap to organise more gentle transformation with smooth shift of highly nonequilibrium states to quasiequilibrium. The following regularisation transformation distributes its action smoothly: we can just choose in (1) $\phi = \phi(\Delta S(f))$ with sufficiently smooth function $\phi(\Delta S(f))$. Here f is the state at some site, f^* is the corresponding quasiequilibrium state, S is entropy, and $\Delta S(f) := S(f^*) - S(f)$.

The next step in the development of the nonequilibrium entropy limiters is in the usage of local entropy filters. The filter of choice here is the median filter: it does not erase sharp fronts, and is much more robust than convolution filters.

An important problem is: “how does one create nonequilibrium entropy limiters for LBM with non-entropic quasiequilibria?”. We propose a solution of this problem based on the nonequilibrium Kullback entropy. For entropic quasiequilibrium the Kullback entropy approach gives the same entropic limiters. In thermodynamics, Kullback entropy belongs to the family of Massieu–Planck–Kramers functions (canonical or grandcanonical potentials).

3 Nonequilibrium entropy limiters for LBM

3.1 Positivity rule

There is a simple recipe for positivity preservation [6,31,41]: to substitute nonpositive $I_0^\beta(f)(\mathbf{x})$ by the closest nonnegative state that belongs to the straight line

$$\left\{ \lambda f(\mathbf{x}) + (1 - \lambda) \Pi^*(f(\mathbf{x})) \mid \lambda \in \mathbb{R} \right\} \quad (5)$$

defined by the two points, $f(\mathbf{x})$ and corresponding quasiequilibrium. This operation is to be applied pointwise, at points of the lattice where positivity is violated. The coefficient λ depends on \mathbf{x} too. Let us call this recipe the *positivity rule* (Fig. 1). This recipe preserves positivity of populations and probabilities, but can affect accuracy of approximation. The same rule is nec-

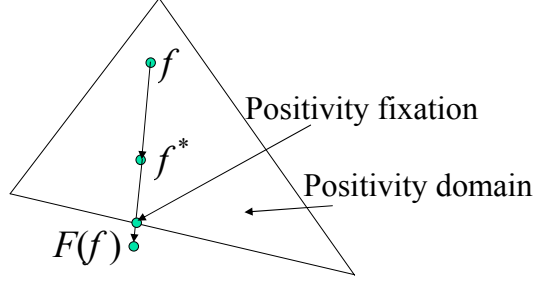


Fig. 1. Positivity rule in action. The motions stops at the positivity boundary.

essary for ELBM (4) when the positive “mirror state” \tilde{f} with the same entropy as f does not exists on the straight line (5).

3.2 Ehrenfests’ regularisation

To discuss methods with additional dissipation, the entropic approach is very convenient. Let entropy $S(f)$ be defined for each population vector $f = (f_i)$ (below we use the same letter S for local in space entropy, and hope that context will make this notation always clear). We assume that the global entropy is a sum of local entropies for all sites. The local nonequilibrium entropy is

$$\Delta S(f) := S(f^*) - S(f), \quad (6)$$

where f^* is the corresponding local quasiequilibrium at the same point.

The *Ehrenfests’ regularisation* [6,7] provides “entropy trimming”: we monitor local deviation of f from the corresponding quasiequilibrium, and when $\Delta S(f)(\mathbf{x})$ exceeds a pre-specified threshold value δ , perform local Ehrenfests’ steps to the corresponding quasiequilibrium: $f \mapsto f^*$ at those points.

So that the Ehrenfests’ steps are not allowed to degrade the accuracy of LBGK it is pertinent to select the k sites with highest $\Delta S > \delta$. The a posteriori estimates of added dissipation could easily be performed by analysis of entropy production in Ehrenfests’ steps. Numerical experiments show (see, e.g., [6,7]) that even a small number of such steps drastically improve stability.

To avoid the change of accuracy order “on average”, the number of sites with this step should be $\leq \mathcal{O}(Nh/L)$ where N is the total number of sites, h is the step of the space discretization and L is the macroscopic characteristic length. But this rough estimate of accuracy in average might be destroyed by concentration of Ehrenfests’ steps in the most nonequilibrium areas, for example, in the boundary layer. In that case, instead of the total number of sites N in $\mathcal{O}(Nh/L)$ we should take the number of sites in a specific region. The effects of concentration could be easily analysed a posteriori.

3.3 Smooth limiters of nonequilibrium entropy

The positivity rule and Ehrenfests' regularisation provide rare, intense and localised corrections. Of course, it is easy and also computationally cheap to organise more gentle transformation with a smooth shift of highly nonequilibrium states to quasiequilibrium. The following regularisation transformation distributes its action smoothly:

$$f \mapsto f^* + \phi(\Delta S(f))(f - f^*). \quad (7)$$

The choice of function ϕ is highly ambiguous, for example, $\phi = 1/(1 + \alpha \Delta S^k)$ for some $\alpha > 0$ and $k > 0$. There are two significantly different choices: (i) ensemble-independent ϕ (i.e., the value of ϕ depends on local value of ΔS only) and (ii) ensemble-dependent ϕ , for example

$$\phi(\Delta S) = \frac{1 + (\Delta S/(\alpha E(\Delta S)))^{k-1/2}}{1 + (\Delta S/(\alpha E(\Delta S)))^k}, \quad (8)$$

where $E(\Delta S)$ is the average value of ΔS in the computational area, $k \geq 1$, and $\alpha \gtrsim 1$. For small ΔS , $\phi(\Delta S) \approx 1$ and for $\Delta S \gg \alpha E(\Delta S)$, $\phi(\Delta S)$ tends to $\sqrt{\alpha E(\Delta S)/\Delta S}$. It is easy to select an ensemble-dependent ϕ with control of total additional dissipation.

3.4 Monitoring of total dissipation

For given β , the entropy production in one LBGK step in quadratic approximation for ΔS is:

$$\delta_{\text{LBGK}} S \approx [1 - (2\beta - 1)^2] \sum_{\mathbf{x}} \Delta S(\mathbf{x}),$$

where \mathbf{x} is the grid point, $\Delta S(\mathbf{x})$ is nonequilibrium entropy (6) at point \mathbf{x} , $\delta_{\text{LBGK}} S$ is the total entropy production in a single LBGK step. It would be desirable if the total entropy production for the limiter $\delta_{\text{lim}} S$ was small relative to $\delta_{\text{LBGK}} S$:

$$\delta_{\text{lim}} S < \delta_0 \delta_{\text{LBGK}} S. \quad (9)$$

A simple ensemble-dependent limiter (perhaps, the simplest one) for a given δ_0 operates as follows. Let us collect the histogram of the $\Delta S(\mathbf{x})$ distribution, and estimate the distribution density, $p(\Delta S)$. We have to estimate a value ΔS_0 that satisfies the following equation:

$$\int_{\Delta S_0}^{\infty} p(\Delta S)(\Delta S - \Delta S_0) d\Delta S = \delta_0 [1 - (2\beta - 1)^2] \int_0^{\infty} p(\Delta S) \Delta S d\Delta S. \quad (10)$$

In order not to affect distributions with small expectation of ΔS , we choose a threshold $\Delta S_t = \max\{\Delta S_0, \delta\}$, where δ is some predefined value (as in the Ehrenfests' regularisation). For states at sites with $\Delta S \geq \Delta S_t$ we provide homothety with quasiequilibrium center f^* and coefficient $\sqrt{\Delta S_t/\Delta S}$ (in quadratic approximation for nonequilibrium entropy):

$$f(\mathbf{x}) \mapsto f^*(\mathbf{x}) + \sqrt{\frac{\Delta S_t}{\Delta S}}(f(\mathbf{x}) - f^*(\mathbf{x})). \quad (11)$$

3.5 Median entropy filter

The limiters described above provide pointwise correction of nonequilibrium entropy at the “most nonequilibrium” points. Due to the pointwise nature, the technique does not introduce any nonisotropic effects, and provides some other benefits. But if we involve the local structure, we can correct local non-monotone irregularities without touching regular fragments. For example, we can discuss monotone increase or decrease of nonequilibrium entropy as regular fragments and concentrate our efforts on reduction of “speckle noise” or “salt and pepper noise”. This approach allows us to use the accessible resource of entropy change (9) more thriftily.

Among all possible filters, we suggest the *median filter*. The median is a more robust average than the mean (or the weighted mean) and so a single very unrepresentative value in a neighborhood will not affect the median value significantly. Hence, we suppose that the median entropy filter will work better than entropy convolution filters.

The median filter considers each site in turn and looks at its nearby neighbours. It replaces the nonequilibrium entropy value ΔS at the point with the median of those values ΔS_{med} , then updates f by the transformation (11) with the homothety coefficient $\sqrt{\Delta S_{\text{med}}/\Delta S}$. The median, ΔS_{med} , is calculated by first sorting all the values from the surrounding neighbourhood into numerical order and then replacing that being considered with the middle value. For example, if a point has 3 nearest neighbors including itself, then after sorting we have 3 values ΔS : $\Delta S_1 \leq \Delta S_2 \leq \Delta S_3$. The median value is $\Delta S_{\text{med}} = \Delta S_2$. For 9 nearest neighbors (including itself) we have after sorting $\Delta S_{\text{med}} = \Delta S_5$. For 27 nearest neighbors $\Delta S_{\text{med}} = \Delta S_{14}$.

We accept only dissipative corrections (those resulting in a decrease of ΔS , $\Delta S_{\text{med}} < \Delta S$) because of the second law of thermodynamics. The analogue of (10) is also useful for acceptance of the most significant corrections.

Median filtering is a common step in image processing [34] for the smoothing of signals and the suppression of impulse noise with preservation of edges.

3.6 Entropic steps for non-entropic quasiequilibria

Beyond the quadratic approximation for nonequilibrium entropy all the logic of the above mentioned constructions remain the same. There exists only one significant change: instead of a simple homothety (11) with coefficient $\sqrt{\Delta S_t/\Delta S}$ the transformation (7) should be applied, where the multiplier ϕ is a solution of the nonlinear equation

$$S(f^* + \phi(f - f^*)) = S(f^*) - \Delta S_t.$$

This is essentially the same equation that appears in the definition of ELBM steps (4).

More differences emerge for LBM with non-entropic quasiequilibria. The main idea here is to reason that non-entropic quasiequilibria appear only because of technical reasons, and approximate continuous physical entropic quasiequilibria. This is not an approximation of a density function, but an approximation of measure, i.e., from the cubature formula:

$$f(\mathbf{v}) \approx \sum_i f_i \delta(\mathbf{v} - \mathbf{v}_i)$$

$$\int \varphi(\mathbf{v}) f(\mathbf{v}) d\mathbf{v} \approx \sum_i \varphi(\mathbf{v}_i) f_i.$$

The discrete populations f_i are connected to continuous (and sufficiently smooth) densities $f(\mathbf{v})$ by cubature weights $f_i \approx w_i f(\mathbf{v}_i)$. These weights for quasiequilibria are found by moment and flux matching conditions [37]. It is impossible to approximate the BGS entropy $\int f \ln f d\mathbf{v}$ just by discretization (to change integration by summation, and continuous distribution f by discrete f_i), because cubature weights appear as additional variables. Nevertheless, the approximate discretization of the Kullback entropy S_K [30] does not change its form:

$$S_K(f) = - \int f(\mathbf{v}) \ln \left(\frac{f(\mathbf{v})}{f^*(\mathbf{v})} \right) d\mathbf{v} \approx - \sum_i f_i \ln \left(\frac{f_i}{f_i^*} \right), \quad (12)$$

because f_i/f_i^* approximates the ratio of functions $f(\mathbf{v})/f^*(\mathbf{v})$ and $\sum_i f_i \dots$ gives the integral $\int f(\mathbf{v}) \dots d\mathbf{v}$ approximation. Here, in (12), the state f^* is the quasiequilibrium with the same values of the macroscopic variables as f . Moreover, for given values of the macroscopic variables, $S_K(f)$ achieves its maximum at the point $f = f^*$ (both for continuous and for discrete distributions). The corresponding maximal value is zero. Below, S_K is the discrete Kullback entropy. If the approximate discrete quasiequilibrium f^* is non-entropic, we can use $-S_K(f)$ instead of $\Delta S(f)$.

For entropic quasiequilibria with perfect entropy the discrete Kullback entropy

gives the same ΔS : $-S_K(f) = \Delta S(f)$. Let the discrete entropy have the standard form for an ideal (perfect) mixture [27].

$$S(f) = - \sum_i f_i \ln \left(\frac{f_i}{W_i} \right).$$

After the classical work of Zeldovich [44], this function is recognised as a useful instrument for the analysis of kinetic equations (especially in chemical kinetics [21]). If we define f^* as the conditional entropy maximum for given $M_j = \sum_k m_{jk} f_k$, then

$$\ln f_k^* = \sum_j \mu_j m_{jk},$$

where $\mu_j(M)$ are the Lagrange multipliers (or “potentials”). For this entropy and conditional equilibrium we find

$$\Delta S = S(f^*) - S(f) = \sum_i f_i \ln \left(\frac{f_i}{f_i^*} \right), \quad (13)$$

if f and f^* have the same moments, $m(f) = m(f^*)$. The right hand side of (13) is $-S_K(f)$.

In thermodynamics, the Kullback entropy belongs to the family of Massieu–Planck–Kramers functions (canonical or grandcanonical potentials). There is another sense of this quantity: S_K is the relative entropy of f with respect to f^* [18,35].

In quadratic approximation,

$$-S_K(f) = \sum_i f_i \ln \left(\frac{f_i}{f_i^*} \right) \approx \sum_i \frac{(f_i - f_i^*)^2}{f_i^*}.$$

3.7 ELBM collisions as a smooth limiter

On the base of numerical tests, the authors of [41] claim that the positivity rule provides the same results (in the sense of stability and absence/presence of spurious oscillations) as the ELBM models, but ELBM provides better accuracy.

For the formal definition of ELBM (4) our tests do not support claims that ELBM erases spurious oscillations (see below). Similar observation for Burgers equation was previously published in [4]. We understand this situation in the following way. The entropic method consists at least of three components:

- (1) entropic quasiequilibrium, defined by entropy maximisation;

- (2) entropy balanced collisions (4) that have to provide proper entropy balance;
- (3) a method for the solution of the transcendental equation $S(f) = S(\tilde{f})$ to find $\alpha = \alpha(f)$ in (4).

It appears that the first two items do not affect spurious oscillations at all, if we solve the equation for $\alpha(f)$ with high accuracy. Additional viscosity is, potentially, added by explicit analytic formulas for $\alpha(f)$. In order not to decrease entropy, errors in these formulas always increase dissipation. This can be interpreted as a hidden transformation of the form (7), where the coefficients in ϕ depend also on f^* .

3.8 Monotonic and double monotonic limiters

Two monotonicity properties are important in the theory of nonequilibrium entropy limiters:

- (1) a limiter should move the distribution to equilibrium: in all cases of (1) $0 \leq \phi \leq 1$. This is the *dissipativity* condition which means that limiters never produce negative entropy.
- (2) a limiter should not change the order of states on the line: if for two distributions with the same moments, f and f' , $\Delta S(f) > \Delta S(f')$ before the limiter transformation, then the same inequality should hold after the limiter transformation too. For example, for the limiter (7) it means that $\Delta S(f^* + x\phi(\Delta S(f^* + x(f - f^*))(f - f^*)))$ is a monotonically increasing function of $x > 0$.

In quadratic approximation,

$$\begin{aligned}\Delta S(f^* + x(f - f^*)) &= x^2 \Delta S(f), \\ \Delta S(f^* + x\phi(\Delta S(f^* + x(f - f^*))(f - f^*))) &= x^2 \phi^2(x^2 \Delta S(f)),\end{aligned}$$

and the second monotonicity condition transforms into the following requirement: $y\phi(y^2 s)$ is a monotonically increasing (not decreasing) function of $y > 0$ for any $s > 0$.

If a limiter satisfies both monotonicity conditions, we call it “double monotonic”. For example, Ehrenfests’ regularisation satisfies the first monotonicity condition, but obviously violates the second one. The limiter (8) violates the first condition for small ΔS , but is dissipative and satisfies the second one in quadratic approximation for large ΔS . The limiter with $\phi = 1/(1 + \alpha \Delta S^k)$ always satisfies the first monotonicity condition, violates the second if $k > 1/2$, and is double monotonic (in quadratic approximation for the second condition), if $0 < k \leq 1/2$. The threshold limiters (11) are also double monotonic.

Of course, it is not forbidden to use any type of limiters under the local and global control of dissipation, but double monotonic limiters provide some natural properties automatically, without additional care.

4 Numerical experiment

To conclude this paper we report some numerical experiments conducted to demonstrate the performance of some of the proposed nonequilibrium entropy limiters for LBM from Sec. 3.

4.1 Velocities and quasiequilibria

We will perform simulations using both entropic and non-entropic quasiequilibria, but we always work with an athermal LBM model. Whenever we use non-entropic quasiequilibria we employ Kullback entropy (13).

In 1D, we use a lattice with spacing and time step $\delta t = 1$ and a discrete velocity set $\{v_1, v_2, v_3\} := \{0, -1, 1\}$ so that the model consists of static, left- and right-moving populations only. The subscript i denotes population (not lattice site number) and f_1 , f_2 and f_3 denote the static, left- and right-moving populations, respectively. The entropy is $S = -H$, with

$$H = f_1 \log(f_1/4) + f_2 \log(f_2) + f_3 \log(f_3),$$

(see, e.g., [27]) and, for this entropy, the local entropic quasiequilibrium state f^* is available explicitly:

$$\begin{aligned} f_1^* &= \frac{2\rho}{3} \left(2 - \sqrt{1 + 3u^2} \right), \\ f_2^* &= \frac{\rho}{6} \left((3u - 1) + 2\sqrt{1 + 3u^2} \right), \\ f_3^* &= -\frac{\rho}{6} \left((3u + 1) - 2\sqrt{1 + 3u^2} \right), \end{aligned} \tag{14}$$

where

$$\rho := \sum_i f_i, \quad u := \frac{1}{\rho} \sum_i v_i f_i. \tag{15}$$

The standard non-entropic polynomial quasiequilibria [38] are:

$$\begin{aligned} f_1^* &= \frac{2\rho}{3} \left(1 - \frac{3u^2}{2} \right), \\ f_2^* &= \frac{\rho}{6} (1 - 3u + 3u^2), \\ f_3^* &= \frac{\rho}{6} (1 + 3u + 3u^2). \end{aligned} \quad (16)$$

In 2D, we employ a uniform 9-speed square lattice with discrete velocities $\{\mathbf{v}_i \mid i = 0, 1, \dots, 8\}$: $\mathbf{v}_0 = 0$, $\mathbf{v}_i = (\cos((i-1)\pi/2), \sin((i-1)\pi/2))$ for $i = 1, 2, 3, 4$, $\mathbf{v}_i = \sqrt{2}(\cos((i-5)\frac{\pi}{2} + \frac{\pi}{4}), \sin((i-5)\frac{\pi}{2} + \frac{\pi}{4}))$ for $i = 5, 6, 7, 8$. The numbering f_0, f_1, \dots, f_8 are for the static, east, north, west, south, north-east, northwest, southwest and southeast-moving populations, respectively. As usual, the entropic quasiequilibrium state, f^* , can be uniquely determined by maximising an entropy functional

$$S(f) = - \sum_i f_i \log \left(\frac{f_i}{W_i} \right),$$

subject to the constraints of conservation of mass and momentum [2]:

$$f_i^* = \rho W_i \prod_{j=1}^2 \left(2 - \sqrt{1 + 3u_j^2} \right) \left(\frac{2u_j + \sqrt{1 + 3u_j^2}}{1 - u_j} \right)^{v_{i,j}}. \quad (17)$$

Here, the *lattice weights*, W_i , are given lattice-specific constants: $W_0 = 4/9$, $W_{1,2,3,4} = 1/9$ and $W_{5,6,7,8} = 1/36$. Analogously to (15), the macroscopic variables ρ and $\mathbf{u} = (u_1, u_2)$ are the zeroth and first moments of the distribution f , respectively. The standard non-entropic polynomial quasiequilibria [38] are:

$$f_i^* = \rho W_i \left(1 + 3\mathbf{v}_i \mathbf{u} + \frac{9(\mathbf{v}_i \mathbf{u})^2}{2} - \frac{3\mathbf{u}^2}{2} \right). \quad (18)$$

4.2 LBGK and ELBM

The governing equations for LBGK are

$$f_i(x + v_i, t + 1) = f_i^*(x, t) + (2\beta - 1)(f_i^*(x, t) - f_i(x, t)), \quad (19)$$

where $\beta = 1/(2\nu + 1)$.

For ELBM (4) the governing equations are:

$$f_i(x + v_i, t + 1) = (1 - \beta)f_i^*(x, t) + \beta \tilde{f}_i(x, t), \quad (20)$$

with β as above and $\tilde{f} = (1 - \alpha)f + \alpha f^*$. The parameter, α , is chosen to satisfy a constant entropy condition. This involves finding the nontrivial root of the equation

$$S((1 - \alpha)f + \alpha f^*) = S(f). \quad (21)$$

To solve (21) numerically we employ a robust routine based on bisection. The root is solved to an accuracy of 10^{-15} and we always ensure that the returned value of α does not lead to a numerical entropy decrease. We stipulate that if, at some site, no nontrivial root of (21) exists we will employ the positivity rule instead (Fig. 1).

4.3 Shock tube

The 1D shock tube for a compressible athermal fluid is a standard benchmark test for hydrodynamic codes. Our computational domain will be the interval $[0, 1]$ and we discretize this interval with 801 uniformly spaced lattice sites. We choose the initial density ratio as 1:2 so that for $x \leq 400$ we set $\rho = 1.0$ else we set $\rho = 0.5$. We will fix the kinematic viscosity of the fluid at $\nu = 10^{-9}$.

4.3.1 Comparison of LBGK and ELBM

In Fig. 2 we compare the shock tube density profile obtained with LBGK (using entropic quasiequilibria (14)) and ELBM. On the same panel we also display both the total entropy $\bar{S}(t) := \sum_x S(x, t)$ and total nonequilibrium entropy $\overline{\Delta S}(t) := \sum_x \Delta S(x, t)$ time histories. As expected, by construction, we observe that total entropy is (effectively) constant for ELBM. On the other hand, LBGK behaves non-entropically for this problem. In both cases we observe that nonequilibrium entropy grows with time.

As we can see, the choice between the two collision formulas LBGK (19) or ELBM (20) does not affect spurious oscillation, and reported regularisation [29] is, perhaps, the result of approximate analytical solution of the equation (21). Inaccuracy in the solution of (21) can be interpreted as a hidden nonequilibrium entropy limiter. But it should be mentioned that the entropic method consists not only of the collision formula, but, what is important, includes a special choice of quasiequilibrium that could improve stability (see, e.g., [13]). Indeed, when we compare ELBM with LBGK using either entropic or standard polynomial quasiequilibria, there appears to be some gain in employing entropic quasiequilibria (Fig. 3). We observe that the post-shock region for the LBGK simulations is more oscillatory when polynomial quasiequilibria are used. In Fig. 3 we have also included a panel with the simulation resulting from a much higher viscosity ($\nu = 3.3333 \times 10^{-2}$). Here, we observe no appreciable differences in the results of LBGK and ELBM.

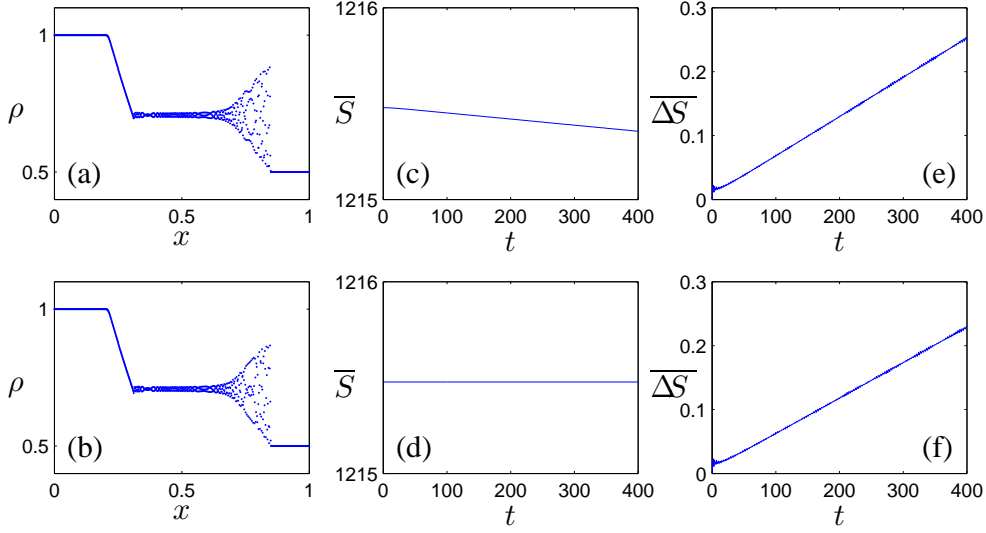


Fig. 2. Density and profile of the 1:2 athermal shock tube simulation with $\nu = 10^{-9}$ after 400 time steps using (a) LBGK (19); (b) ELBM (20). In this example, no negative population are produced by any of the methods so the positivity rule is redundant. For ELBM in this example, (21) always has a nontrivial root. Total entropy and nonequilibrium entropy time histories are shown in panels (c), (d) and (e), (f) for LBGK and ELBM, respectively.

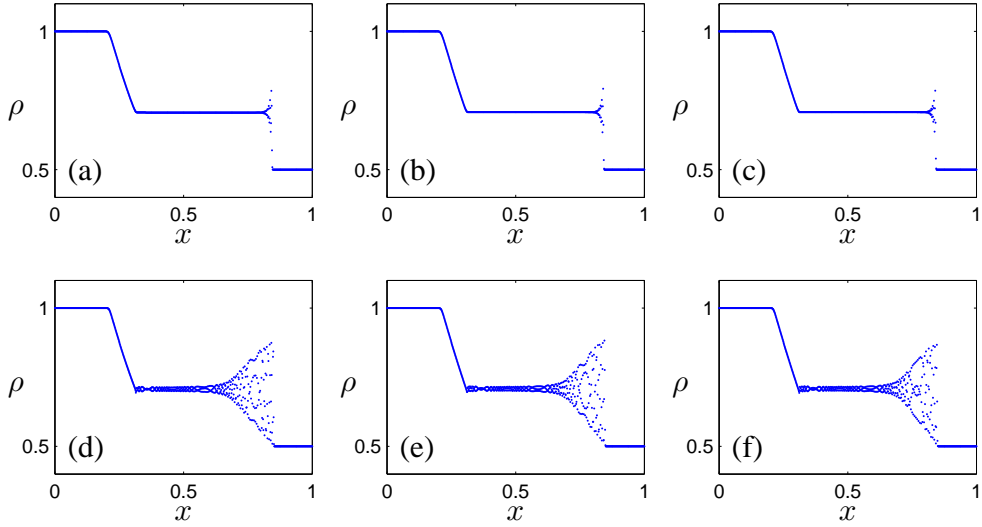


Fig. 3. Density and velocity profile of the 1:2 isothermal shock tube simulation after 400 time steps using (a) LBGK (19) with polynomial quasiequilibria (16) [$\nu = 3.3333 \times 10^{-2}$]; (b) LBGK (19) with entropic quasiequilibria (14) [$\nu = 3.3333 \times 10^{-2}$]; (c) ELBM (20) [$\nu = 3.3333 \times 10^{-2}$]; (d) LBGK (19) with polynomial quasiequilibria (16) [$\nu = 10^{-9}$]; (e) LBGK (19) with entropic quasiequilibria (14) [$\nu = 10^{-9}$]; (f) ELBM (20) [$\nu = 10^{-9}$].

4.3.2 Nonequilibrium entropy limiters.

Now, we would like to demonstrate just a representative sample of the many possibilities of limiters suggested in Sec. 3. In each case the limiter is implemented by a post-processing routine immediately following the collision step (either LBGK (19) or ELBM (20)). Here, we will only consider LBGK collisions and entropic quasiequilibria (14).

The post-processing step adjusts f by the update formula:

$$f \mapsto f^* + \phi(\Delta S)(f - f^*),$$

where ΔS is defined by (6) and ϕ is a limiter function.

For the Ehrenfests' regularisation one would choose

$$\phi(\Delta S)(x) = \begin{cases} 1, & \Delta S(x) \leq \delta, \\ 0, & \text{otherwise,} \end{cases}$$

where δ is a pre-specified threshold value. Furthermore, it is pertinent to select just k sites with highest $\Delta S > \delta$. This limiter has been previously applied to the shock tube problem in [6,7,8] and we will not reproduce those results here.

Instead, our first example will be the following smooth limiter:

$$\phi(\Delta S) = \frac{1}{1 + \alpha \Delta S^k}. \quad (22)$$

For this limiter, we will fix $k = 1/2$ (so that the limiter is double monotonic in quadratic approximation to entropy) and compare the density profiles for $\alpha = \delta/(E(\Delta S)^k)$, $\delta = 0.1, 0.01, 0.001$. We have also ensured an ensemble-dependent limiter because of the dependence of α on the average $E(\Delta S)$. As with Fig. 2, we accompany each panel with the total entropy and nonequilibrium entropy histories. Note the different scales for nonequilibrium entropy. Note also that entropy (necessarily) now grows due to the additional dissipation.

Our next example (Fig. 5) considers the threshold filter (10). In this example we choose the estimates $\Delta S_0 = 5E(\Delta S), 10E(\Delta S), 20E(\Delta S)$ and fix the tolerance $\delta = 0$ so that the influence of the threshold alone can be studied. Only entropic adjustments are accepted in the limiter: $\Delta S_t \leq \Delta S$. As the threshold increases, nonequilibrium entropy grows faster and spurious begin to appear.

Finally, we test the median filter (Fig. 6). We choose a minimal filter so that only the nearest neighbours are considered. As with the threshold filter, we introduce a tolerance δ and we try the values $\delta = 10^{-3}, 10^{-4}, 10^{-5}$. Only entropic adjustments are accepted in the limiter: $\Delta S_{\text{med}} \leq \Delta S$.

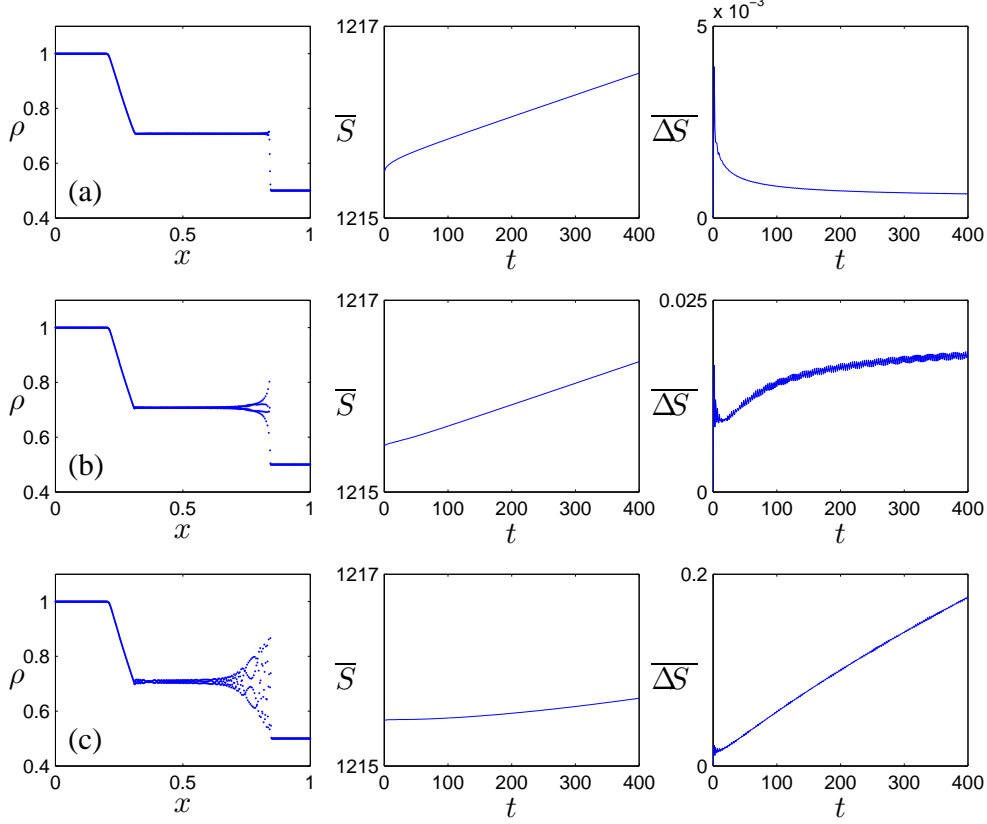


Fig. 4. Density and profile of the 1:2 athermal shock tube simulation with $\nu = 10^{-9}$ after 400 time steps using LBGK (19) and the smooth limiter (22) with $k = 1/2$, $\alpha = \delta/(E(\Delta S)^k)$ and (a) $\delta = 0.1$; (b) $\delta = 0.01$ and (c) $\delta = 0.001$. Total entropy and nonequilibrium entropy time histories for each parameter set $\{k, \alpha(\delta)\}$ are displayed in the adjacent panels.

We have seen that each of the examples we have considered (Fig. 4, Fig. 5 and Fig. 6) is capable of subduing spurious post-shock oscillations compared with LBGK (or ELBM) on this problem (cf. Fig. 2). Of course, by limiting nonequilibrium entropy the result is necessarily an increase in entropy.

From our experiences our recommendation is that the median filter is the superior choice amongst all the limiters suggested in Sec. 3. The action of the median filter is found to be both extremely gentle and, at the same time, very effective.

4.4 Lid-driven cavity

Our second numerical example is the classical 2D lid-driven cavity flow. A square cavity of side length L is filled with fluid with kinematic viscosity ν (initially at rest) and driven by the cavity lid moving at a constant velocity $(u_0, 0)$ (from left to right in our geometry).

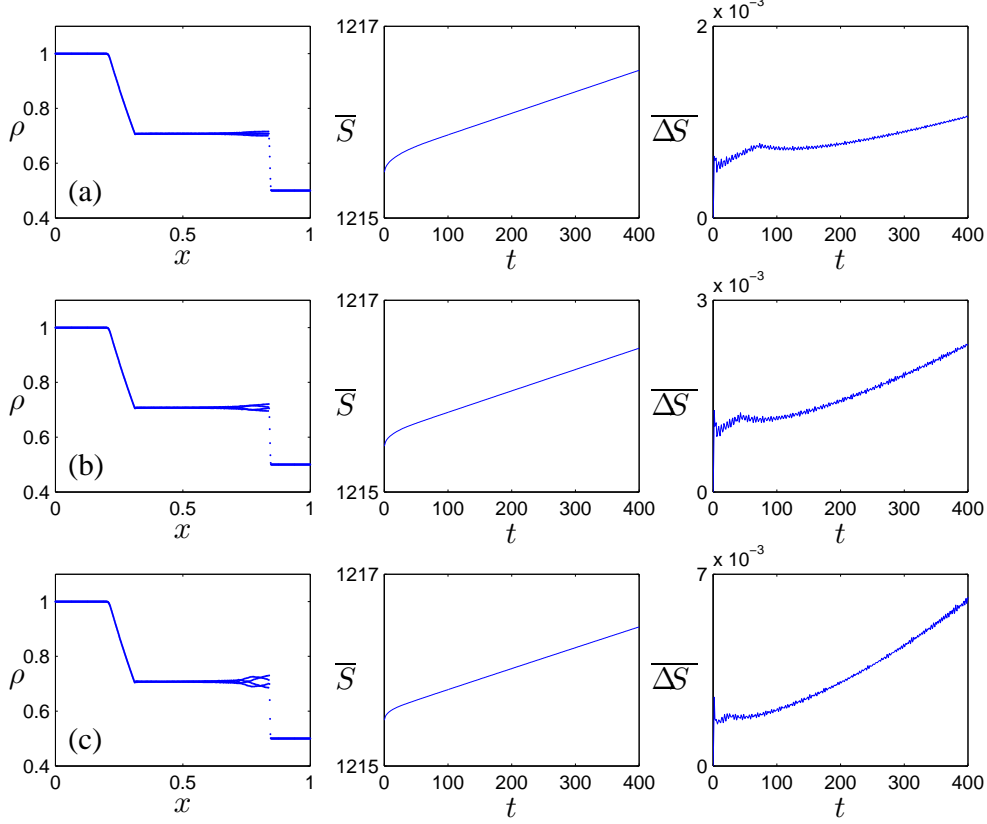


Fig. 5. Density and profile of the 1:2 athermal shock tube simulation with $\nu = 10^{-9}$ after 400 time steps using LBGK (19) and the threshold limiter (10) with (a) $\Delta S_t = 5E(\Delta S)$; (b) $\Delta S_t = 10E(\Delta S)$ and (c) $\Delta S_t = 20E(\Delta S)$. Total entropy and nonequilibrium entropy time histories for each threshold ΔS_t are displayed in the adjacent panels.

We will simulate the flow on a 100×100 grid using LBGK regularised with the median filter limiter. Unless otherwise stated, we use entropic quasiequilibria (17). The implementation of the filter is as follows: the filter is not applied to boundary nodes; for nodes which immediately neighbour the boundary the stencil consists of the 3 nearest neighbours (including itself) closest to the boundary; for all other nodes the minimal stencil of 9 nearest neighbours is used.

We have purposefully selected such a coarse grid simulation because it is readily found that, on this problem, unregularised LBGK fails (blows-up) for all but the most modest Reynolds numbers $\text{Re} := Lu_0/\nu$.

4.4.1 Steady-state vortex centres

For modest Reynolds number the system settles to a steady state in which the dominant features are a primary central rotating vortex, with several counter-rotating secondary vortices located in the bottom-left, bottom-right (and pos-

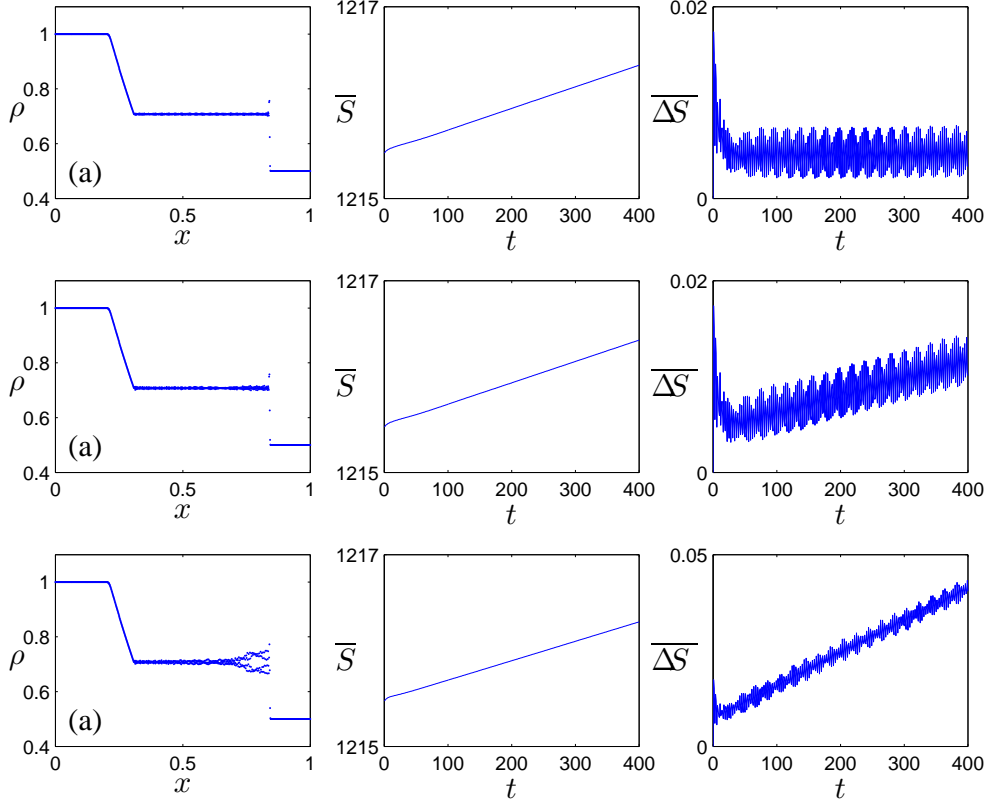


Fig. 6. Density and profile of the 1:2 athermal shock tube simulation with $\nu = 10^{-9}$ after 400 time steps using LBGK (19) and the minimal median limiter with (a) $\delta = 10^{-5}$; (b) $\delta = 10^{-4}$ and (c) $\delta = 10^{-3}$. Total entropy and nonequilibrium entropy time histories for each tolerance δ are displayed in the adjacent panels.

sibly top-left) corners.

Steady state has been extensively investigated in the literature. The study of Hou et al [24] simulates the flow over a range of Reynolds numbers using unregularised LBGK on a 256×256 grid. Primary and secondary vortex centre data is provided. We compare this same statistic for the present median filtered coarse grid simulation. We will employ the same convergence criteria used in [24]. Namely, we deem that steady state has been reached by ensuring that the difference between the maximum value of the stream function for successive 10,000 time steps is less than 10^{-5} . The stream function, which is not a primary variable in the LBM simulation, is obtained from the velocity data by integration using Simpson’s rule. Vortex centres are characterised as local extrema of the stream function.

We compare our results with the LBGK simulations in [24] and [41]. To align ourselves with these studies we specify the following boundary condition: lid profile is constant; remaining cavity walls are subject to the “bounce-back” condition [38]. In our simulations, the initial uniform fluid density profile is $\rho = 2.7$ and the velocity of the lid is $u_0 = 1/10$ (in lattice units).

Collected in Table 1, for $Re = 2000, 5000$ and 7500 , are the coordinates of the primary and secondary vortex centres using (a) unregularised LBGK; (b) LBGK with median filter limiter ($\delta = 10^{-3}$); (c) LBGK with median filter limiter ($\delta = 10^{-4}$), all with non-entropic polynomial quasiequilibria (18). Lines (d), (e) and (f) are the same but with entropic quasiequilibria (17). The remaining lines of Table 1 are as follows: (g) literature data [24] (unregularised LBGK on a 256×256 grid); (h) literature data [41] (positivity rule); (i) literature data [41] (ELBM). With the exception of (g), all simulation are conducted on a 100×100 grid. The top-left vortex does not appear at $Re = 2000$ and no data was provided for it in [41] at $Re = 5000$. The unregularised LBGK $Re = 7500$ simulation blows-up in finite time and the simulation becomes meaningless. The y -coordinate of the two lower-vortices at $Re = 5000$ in (i) appear anomalously small and were not reproduced by our experiments with the positivity rule (not shown).

We have conducted two runs of the experiment with the median filter parameter $\delta = 10^{-3}$ and $\delta = 10^{-4}$. Despite the increased number of realisations the vortex centre locations remain effectively unchanged and we detect no significant variation between the two runs. This demonstrates the gentle nature of the median filter. At Reynolds $Re = 2000$ the median filter has no effect at all on the vortex centres compared with LBGK.

We find no significant differences between the experiments with entropic and non-entropic polynomial quasiequilibria in this test.

The coordinates of the primary vortex centre for unregularised LBGK at $Re = 5000$ are already quite inaccurate as LBGK begins to lose stability. Stability is lost entirely at some critical Reynolds number $5000 < Re \leq 7500$ and the simulation blows-up.

Furthermore, we have agreement (within grid resolution) with the data given in [24]. Also compiled in Table 1 is the data from the limiter experiments conducted in [41] (although not explicitly discussed in the language of limiters by the authors of that work). In [41] the authors give vortex centre data for the positivity rule (Fig. 1) and for ELBM (which we interpret as containing a hidden limiter). In [41] the positivity rule is called FIX-UP.

As Reynolds number increases the flow in the cavity is no longer steady and a more complicated flow pattern emerges. On the way to a fully developed turbulent flow, the lid-driven cavity flow is known to undergo a series of period doubling Hopf bifurcations. On our coarse grid, we observe that the coordinates of the primary vortex centre (maximum of the stream function) is a very robust feature of the flow, with little change between coordinates (no change in y -coordinates) computed at $Re = 5000$ and $Re = 7500$ with the median filter. On one hand, because of this observation it becomes inconclusive whether

Table 1

Primary and secondary vortex centre coordinates for the lid-driven cavity flow at $Re = 2000, 5000, 7500$.

Re		Primary		Lower-left		Lower-right		Top-left	
		x	y	x	y	x	y	x	y
2000	(a)	0.5253	0.5455	0.0909	0.1010	0.8384	0.1010	Not applicable	
2000	(b)	0.5253	0.5455	0.0909	0.1010	0.8384	0.1010	Not applicable	
2000	(c)	0.5253	0.5455	0.0909	0.1010	0.8384	0.1010	Not applicable	
2000	(d)	0.5253	0.5455	0.0909	0.1010	0.8384	0.1010	Not applicable	
2000	(e)	0.5253	0.5455	0.0909	0.1010	0.8384	0.1010	Not applicable	
2000	(f)	0.5253	0.5455	0.0909	0.1010	0.8384	0.1010	Not applicable	
2000	(g)	0.5255	0.5490	0.0902	0.1059	0.8471	0.0980	Not applicable	
2000	(h)	0.5200	0.5450	0.0900	0.1000	0.8300	0.0950	Not applicable	
2000	(i)	0.5200	0.5500	0.0890	0.1000	0.8300	0.1000	Not applicable	
5000	(a)	0.5152	0.6061	0.0808	0.1313	0.7980	0.0707	0.0505	0.8990
5000	(b)	0.5152	0.5354	0.0808	0.1313	0.8081	0.0808	0.0606	0.8990
5000	(c)	0.5152	0.5354	0.0808	0.1313	0.8081	0.0808	0.0707	0.8889
5000	(d)	0.5152	0.5960	0.0808	0.1313	0.8081	0.0808	0.0505	0.8990
5000	(e)	0.5152	0.5354	0.0808	0.1313	0.8081	0.0808	0.0606	0.8990
5000	(f)	0.5152	0.5354	0.0808	0.1313	0.8081	0.0808	0.0707	0.8889
5000	(g)	0.5176	0.5373	0.0784	0.1373	0.8078	0.0745	0.0667	0.9059
5000	(h)	0.5150	0.5680	0.0950	0.0100	0.8450	0.0100	Not available	
5000	(i)	0.5150	0.5400	0.0780	0.1350	0.8050	0.0750	Not available	
7500	(a)	—	—	—	—	—	—	—	—
7500	(b)	0.5051	0.5354	0.0707	0.1515	0.7879	0.0707	0.0606	0.8990
7500	(c)	0.5051	0.5354	0.0707	0.1515	0.7879	0.0707	0.0707	0.8889
7500	(d)	—	—	—	—	—	—	—	—
7500	(e)	0.5051	0.5354	0.0707	0.1515	0.7879	0.0707	0.0606	0.8990
7500	(f)	0.5051	0.5354	0.0707	0.1515	0.7879	0.0707	0.0707	0.8889
7500	(g)	0.5176	0.5333	0.0706	0.1529	0.7922	0.0667	0.0706	0.9098

the median limiter is adding too much additional dissipation. On the other hand, a more studious choice of control criteria may indicate that the first bifurcation has already occurred by $\text{Re} = 7500$.

4.4.2 First Hopf bifurcation

A survey of available literature reveals that the precise value of Re at which the first Hopf bifurcation occurs is somewhat contentious, with most current studies (all of which are for incompressible flow) ranging from around $\text{Re} = 7400$ – 8500 [9,32,33]. Here, we do not intend to give a precise value because it is a well observed grid effect that the critical Reynolds number increases (shifts to the right) with refinement (see, e.g., Fig. 3 in [33]). Rather, we will be content to localise the first bifurcation and, in doing so, demonstrate that limiters are capable of regularising without effecting fundamental flow features.

To localise the first bifurcation we take the following algorithmic approach. Entropic quasiequilibria are in use. The initial uniform fluid density profile is $\rho = 1.0$ and the velocity of the lid is $u_0 = 1/10$ (in lattice units). We record the unsteady velocity data at a single control point with coordinates $(L/16, 13L/16)$ and run the simulation for 5000 non-dimensional time units ($5000L/u_0$ time steps). Let us denote the final 1% of this signal by $(u_{\text{sig}}, v_{\text{sig}})$. We then compute the *energy* E_u (ℓ_2 -norm normalised by non-dimensional signal duration) of the deviation of u_{sig} from its mean:

$$E_u := \left\| \sqrt{\frac{L}{u_0|u_{\text{sig}}|}} (u_{\text{sig}} - \overline{u_{\text{sig}}}) \right\|_{\ell_2}, \quad (23)$$

where $|u_{\text{sig}}|$ and $\overline{u_{\text{sig}}}$ denote the length and mean of u_{sig} , respectively. We choose this robust statistic instead of attempting to measure signal amplitude because of numerical noise in the LBM simulation. The source of noise in LBM is attributed to the existence of an inherently unavoidable neutral stability direction in the numerical scheme (see, e.g., [8]).

We opt not to employ the “bounce-back” boundary condition used in the previous steady state study. Instead we will use the diffusive Maxwell boundary condition (see, e.g., [11]), which was first applied to LBM in [1]. The essence of the condition is that populations reaching a boundary are reflected, proportional to equilibrium, such that mass-balance (in the bulk) and detail-balance are achieved. The boundary condition coincides with “bounce-back” in each corner of the cavity.

To illustrate, immediately following the advection of populations consider the situation of a wall, aligned with the lattice, moving with velocity u_{wall} and with outward pointing normal to the wall in the negative y -direction (this is

the situation on the lid of the cavity with $u_{\text{wall}} = u_0$). The implementation of the diffusive Maxwell boundary condition at a boundary site (x, y) on this wall consists of the update

$$f_i(x, y, t + 1) = \gamma f_i^*(u_{\text{wall}}), \quad i = 4, 7, 8,$$

with

$$\gamma = \frac{f_2(x, y, t) + f_5(x, y, t) + f_6(x, y, t)}{f_4^*(u_{\text{wall}}) + f_7^*(u_{\text{wall}}) + f_8^*(u_{\text{wall}})}.$$

Observe that, because density is a linear factor of the quasiequilibria (17), the density of the wall is inconsequential in the boundary condition and can therefore be taken as unity for convenience. As is usual, only those populations pointing in to the fluid at a boundary site are updated. Boundary sites do not undergo the collisional step that the bulk of the sites are subjected to.

We prefer the diffusive boundary condition over the often preferred “bounce-back” boundary condition with constant lid profile. This is because we have experienced difficulty in separating the aforementioned numerical noise from the genuine signal at a single control point using “bounce-back”. We remark that the diffusive boundary condition does not prevent unregularised LBGK from failing at some critical Reynolds number $\text{Re} > 5000$.

Now, we conduct an experiment and record (23) over a range of Reynolds numbers. In each case the median filter limiter is employed with parameter $\delta = 10^{-3}$. Since the transition between steady and periodic flow in the lid-driven cavity is known to belong to the class of standard Hopf bifurcations we are assured that $E_u^2 \propto \text{Re}$ [16]. Fitting a line of best fit to the resulting data localises the first bifurcation in the lid-driven cavity flow to $\text{Re} = 7135$ (Fig. 7). This value is within the tolerance of $\text{Re} = 7402 \pm 4\%$ given in [33] for a 100×100 grid. We also provide a (time averaged) phase space trajectory and Fourier spectrum for $\text{Re} = 7375$ at the monitoring point (Fig. 8 and Fig. 9) which clearly indicate that the first bifurcation has been observed.

5 Conclusions

Entropy and thermodynamics are important for stability of the lattice Boltzmann methods. It is now clear: after almost 10 years of work since the publication of [26] proved this statement (the main reviews are [5,28,39]). The question is now: “how does one utilise, optimally, entropy and thermodynamic structures in lattice Boltzmann methods?”. In our paper we attempt to propose a solution (temporary, at least). Our approach is applicable to both entropic as well as for non-entropic polynomial quasiequilibria.

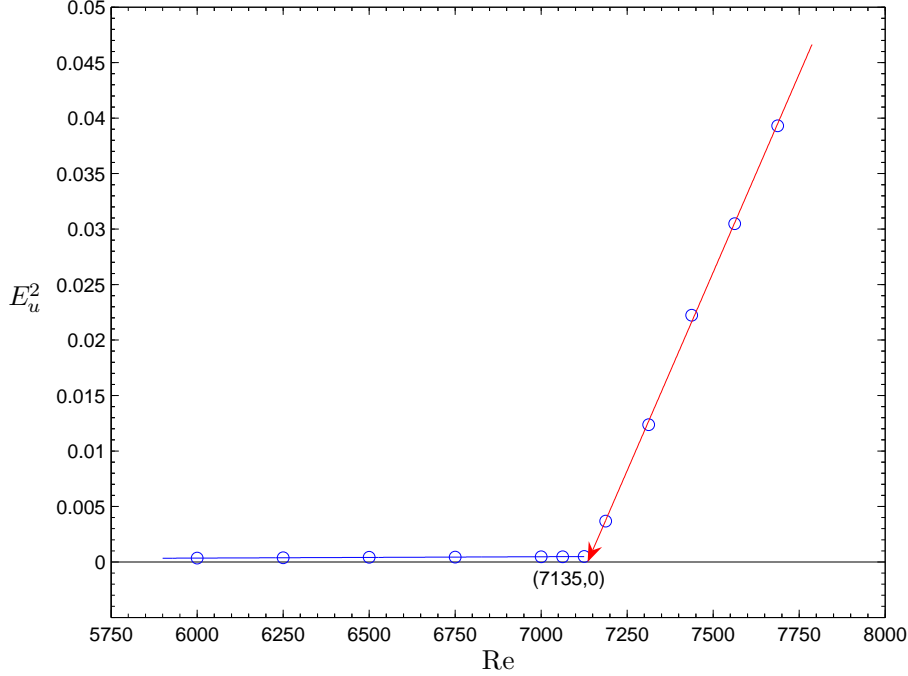


Fig. 7. Plot of energy squared, E_u^2 (23), as a function of Reynolds number, Re , using LBGK regularised with the median filter limiter with $\delta = 10^{-3}$ on a 100×100 grid. Straight lines are lines of best fit. The intersection of the sloping line with the x -axis occurs close to $Re = 7135$.

We have constructed a system of nonequilibrium entropy limiters for the lattice Boltzmann methods (LBM):

- the positivity rule that provides positivity of distribution;
- the pointwise entropy limiters based on selection and correction of most nonequilibrium values;
- filters of nonequilibrium entropy, and the median filter as a filter of choice.

All these limiters exploit physical properties of LBM and allow control of total additional entropy production. In general, they do the same work for LBM as flux limiters do for finite differences, finite volumes and finite elements methods, and come into operation when sharp gradients are present. For smoothly changing waves, the limiters do not operate and the spatial derivatives can be represented by higher order approximations without introducing non-physical oscillations. But there are some differences too: for LBM the main idea behind the construction of nonequilibrium entropy limiter schemes is to limit a scalar quantity — the nonequilibrium entropy — or to delete the “salt and pepper” noise from the field of this quantity. We do not touch the vectors or tensors of spatial derivatives, as it is for flux limiters.

Standard test examples demonstrate that the developed limiters erase spurious oscillations without blurring of shocks, and do not affect smooth solutions. The limiters we have tested do not produce a noticeable additional dissipation and

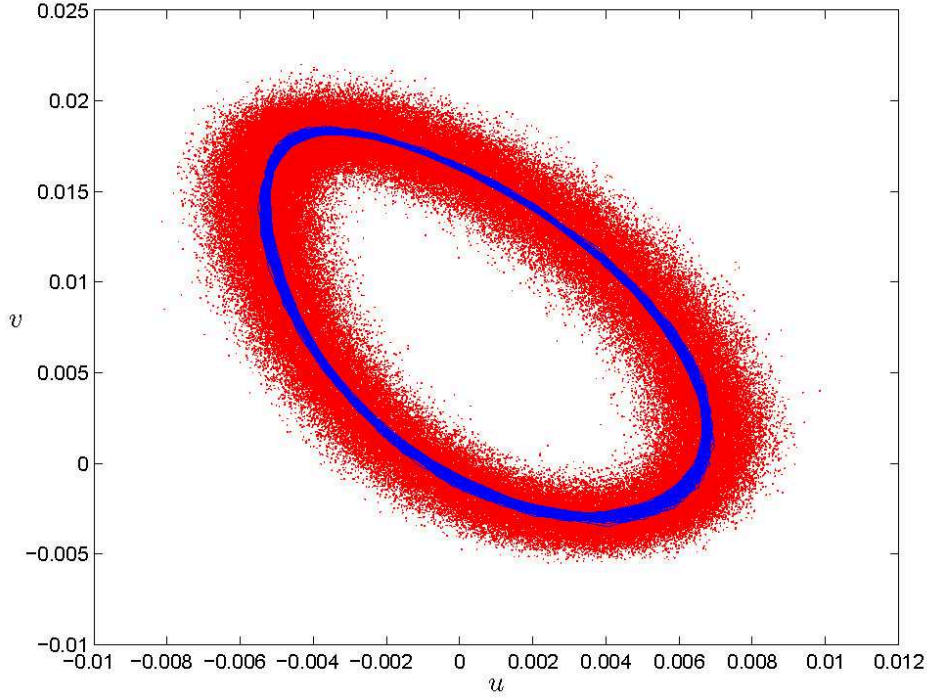


Fig. 8. Velocity components as a function of time for the signal $(u_{\text{sig}}, v_{\text{sig}})$ at the monitoring point $(L/16, 13L/16)$ using LBGK regularised with the median filter limiter with $\delta = 10^{-3}$ on a 100×100 grid ($\text{Re} = 7375$). Dots represent simulation results and the solid line is a 100 step time average of the signal.

allow us to reproduce the first Hopf bifurcation for 2D lid-driven cavity on a coarse 100×100 grid. At the same time the simplest median filter deletes the spurious post-shock oscillations for low viscosity.

Perhaps, it is impossible to find one best nonequilibrium entropy limiter for all problems. It is a special task to construct the optimal limiters for a specific classes of problems.

Acknowledgments

Discussion of the preliminary version of this work with S. Succi and participants of the lattice Boltzmann workshop held on 15th November 2006 in Leicester (UK) was very important. Author A. N. Gorban is grateful to S. K. Godunov for the course of numerical methods given many years ago at Novosibirsk University. This work is supported by Engineering and Physical Sciences Research Council (EPSRC) grant number GR/S95572/01.

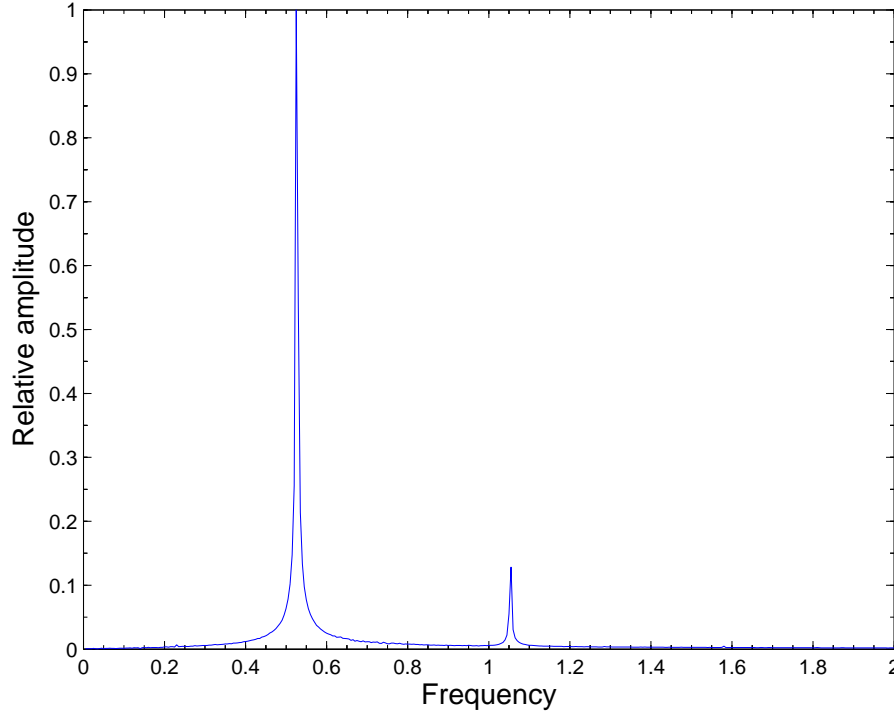


Fig. 9. Relative amplitude spectrum for the signal u_{sig} at the monitoring point $(L/16, 13L/16)$ using LBGK regularised with the median filter limiter with $\delta = 10^{-3}$ on a 100×100 grid ($\text{Re} = 7375$). We measure a dominant frequency of $\omega = 0.525$.

References

- [1] S. Ansumali, and I. V. Karlin. Kinetic boundary conditions in the lattice Boltzmann method. *Phys. Rev. E* **66**, 026311 2002.
- [2] S. Ansumali S, I. V. Karlin, H. C. Ottinger. Minimal entropic kinetic models for hydrodynamics *Europhys. Let.* 63 (6): 798-804. 2003
- [3] R. Benzi, S. Succi, and M. Vergassola. The lattice Boltzmann-equation - theory and applications. *Physics Reports*, 222(3):145–197, 1992.
- [4] B. M. Boghosian, P. J. Love, and J. Yepéz. Entropic lattice Boltzmann model for Burgers equation. *Phil. Trans. Roy. Soc. A*, 362:1691–1702, 2004.
- [5] B. M. Boghosian, J. Yepéz, P. V. Coveney, and A. J. Wager. Entropic lattice Boltzmann methods. *R. Soc. Lond. Proc. Ser. A Math. Phys. Eng. Sci.*, 457(2007):717–766, 2001.
- [6] R. A. Brownlee, A. N. Gorban, and J. Levesley. Stabilisation of the lattice-Boltzmann method using the Ehrenfests’ coarse-graining. *cond-mat/0605359*, 2006.
- [7] R. A. Brownlee, A. N. Gorban, and J. Levesley. Stabilisation of the lattice-Boltzmann method using the Ehrenfests’ coarse-graining. *Phys. Rev. E*, 74:037703, 2006.

- [8] R. A. Brownlee, A.N. Gorban, and J. Levesley. Stability and stabilization of the lattice Boltzmann method, *Phys. Rev. E*, to appear. *cond-mat/0611444*, 2006.
- [9] C.-H. Bruneau, and M. Saad. The 2D lid-driven cavity problem revisited. *Comput. Fluids*, 35:326–348, 2006.
- [10] S. R. Chatkravathy, and S. Osher. High resolution applications of the Osher upwind scheme for the Euler equations, AIAA Paper 83-1943, Proc. AIAA 6th Computational Fluid Dynamics Conference, (1983), 363–373.
- [11] C. Cercignani. *Theory and Application of the Boltzmann Equation*. Scottish Academic Press, Edinburgh, 1975.
- [12] S. Chen and G. D. Doolen. Lattice Boltzmann method for fluid flows. *Annu. Rev. Fluid. Mech.*, 30:329–364, 1998.
- [13] S. S. Chikatamarla and I. V. Karlin. Entropy and Galilean Invariance of Lattice Boltzmann Theories. *Phys. Rev. Lett.* 97, 190601 (2006)
- [14] A. J. Chorin, O. H. Hald, R. Kupferman. Optimal prediction with memory, *Physica D* 166 (2002), 239–257.
- [15] P. Ehrenfest and T. Ehrenfest. *The conceptual foundations of the statistical approach in mechanics*. Dover Publications Inc., New York, 1990.
- [16] N. K. Ghaddar, K. Z. Korczak, B. B. Mikic, and A. T. Patera. Numerical investigation of incompressible flow in grooved channels. Part 1. Stability and self-sustained oscillations. *J. Fluid Mech.*, 163:99–127, 1986.
- [17] S. K. Godunov. A Difference Scheme for Numerical Solution of Discontinuous Solution of Hydrodynamic Equations, *Math. Sbornik*, 47 (1959), 271–306.
- [18] A. N. Gorban. Equilibrium encircling. Equations of chemical kinetics and their thermodynamic analysis, Nauka, Novosibirsk, 1984.
- [19] A. N. Gorban, I. V. Karlin, H. C. Öttinger, and L. L. Tatarinova. Ehrenfest’s argument extended to a formalism of nonequilibrium thermodynamics. *Phys. Rev. E*, 62:066124, 2001.
- [20] A. N. Gorban. Basic types of coarse-graining. In A. N. Gorban, N. Kazantzis, I. G. Kevrekidis, H.-C. Öttinger, and C. Theodoropoulos, editors, *Model Reduction and Coarse-Graining Approaches for Multiscale Phenomena*, pages 117–176. Springer, Berlin-Heidelberg-New York, 2006. *cond-mat/0602024*.
- [21] A. Gorban, B. Kaganovich, S. Filippov, A. Keiko, V. Shamansky, I. Shirkalin, *Thermodynamic Equilibria and Extrema: Analysis of Attainability Regions and Partial Equilibrium*, Springer, Berlin, Heidelberg, New York, 2006.
- [22] H. Grad. On the kinetic theory of rarefied gases, *Comm. Pure and Appl. Math.* 2 4, (1949), 331–407.
- [23] F. Higuera, S. Succi, and R. Benzi. Lattice gas – dynamics with enhanced collisions. *Europhys. Lett.*, 9:345–349, 1989.

- [24] S. Hou, Q. Zou, S. Chen, G. Doolen and A. C. Cogley. Simulation of cavity flow by the lattice Boltzmann method. *J. Comp. Phys.*, 118:329–347, 1995.
- [25] D. Jou, J. Casas-Vázquez, G. Lebon. *Extended irreversible thermodynamics*, Springer, Berlin, 1993.
- [26] I. V. Karlin, A. N. Gorban, S. Succi, and V. Boffi. Maximum entropy principle for lattice kinetic equations. *Phys. Rev. Lett.*, 81:6–9, 1998.
- [27] I. V. Karlin, A. Ferrante, and H. C. Öttinger. Perfect entropy functions of the lattice Boltzmann method. *Europhys. Lett.*, 47:182–188, 1999.
- [28] I. V. Karlin, S. Ansumali, C. E. Frouzakis, and S. S. Chikatamarla. Elements of the lattice Boltzmann method I: Linear advection equation. *Commun. Comput. Phys.*, 1 (2006), 616–655.
- [29] I. V. Karlin, S. S. Chikatamarla and S. Ansumali. Elements of the lattice Boltzmann method II: Kinetics and hydrodynamics in one dimension. *Commun. Comput. Phys.*, 2 (2007), 196–238.
- [30] S. Kullback. *Information theory and statistics*, Wiley, New York, 1959.
- [31] Y. Li, R. Shock, R. Zhang, and H. Chen. Numerical study of flow past an impulsively started cylinder by the lattice-Boltzmann method. *J. Fluid Mech.*, 519:273–300, 2004.
- [32] T. W. Pan, and R. Glowinski. A projection/wave-like equation method for the numerical simulation of incompressible viscous fluid flow modeled by the Navier–Stokes equations. *Comp. Fluid Dyn. J.*, 9:28–42, 2000.
- [33] Y.-F. Peng, Y.-H. Shiau, and R. R. Hwang. Transition in a 2-D lid-driven cavity flow. *Comput. Fluids*, 32:337–352, 2003.
- [34] W. K. Pratt. *Digital Image Processing*, Wiley, New York, 1978.
- [35] H. Qian. Relative entropy: free energy associated with equilibrium fluctuations and nonequilibrium deviations, *Phys. Rev. E*. 63 (2001), 042103.
- [36] P. L. Roe. Characteristic-based schemes for the Euler equations, *Ann. Rev. Fluid Mech.*, 18 (1986), 337–365.
- [37] X. Shan, X-F. Yuan, and H. Chen. Kinetic theory representation of hydrodynamics: a way beyond the NavierStokes equation. *J. Fluid Mech.* 550 (2006), 413–441.
- [38] S. Succi. *The lattice Boltzmann equation for fluid dynamics and beyond*. Oxford University Press, New York, 2001.
- [39] S. Succi, I. V. Karlin, and H. Chen. Role of the H theorem in lattice Boltzmann hydrodynamic simulations. *Rev. Mod. Phys.*, 74:1203–1220, 2002.
- [40] P. K. Sweby. High resolution schemes using flux-limiters for hyperbolic conservation laws. *SIAM J. Num. Anal.*, 21 (1984), 995–1011.

- [41] F. Tosi, S. Ubertini, S. Succi, H. Chen, and I.V. Karlin. Numerical stability of entropic versus positivity-enforcing lattice Boltzmann schemes. *Math. Comput. Simulation*, 72:227–231, 2006.
- [42] B. Van Leer. Towards the ultimate conservative difference scheme III. Upstream-centered finite-difference schemes for ideal compressible flow., *J. Comp. Phys.*, 23 (1977), 263–275.
- [43] P. Wesseling. Principles of Computational Fluid Dynamics, Springer Series in Computational Mathematics (Springer-Verlag, Berlin, 2001), Vol. 29.
- [44] Y. B. Zeldovich, Proof of the Uniqueness of the Solution of the Equations of the Law of Mass Action, In: *Selected Works of Yakov Borisovich Zeldovich*, Vol. 1, J. P. Ostriker (Ed.), Princeton University Press, Princeton, USA, 1996, 144–148.